Comp. Fluid Dyn., 1995, Vol. 4, p. 57–71
Reprints available directly from the publisher
Photocopying permitted by license only

ANALYSIS OF COMBUSTION PROCESSES IN A GUN INTERIOR BALLISTICS

T. W. H. SHEU and S.-M. LEE

Institute of Naval Architecture and Ocean Engineering, National Taiwan University, Taipei, Taiwan, R.O.C.

SUMMARY

This paper presents the numerical simulation of the gas–solid combustion physics in a gun tube with a mobile projectile by means of a flux-corrected transport nonlinear filtering scheme. The analysis is based on a one-dimensional formulation of the two-phase flowfield with the space-sharing interspersed continuum assumption. Apart from the Nobel-Abel equation of state account the interphase drag and intergranular stress between the solid–gas phase are taken into account. The computer code has been used effectively to study the pressure-wave propagation and flame dynamics in a gun barrel containing granular solid propellants.

KEY WORDS: Gas–solid, mobile projectile, flux-corrected transport, combustion.

1. INTRODUCTION

The gun-interior ballistics involves many intricate physical and chemical processes. Investigation of such phenomena is difficult to perform experimentally and subject to a high degree of uncertainty and inaccuracy. Recent advances in computer hardware and solution algorithms have made the numerical study of the two-phase gun interior ballistics possible.

The major physical processes involved in a gun interior ballistics during the transient period were well described by Kuo.[1] The chemical processes following the ignition of the solid propellant usually occur within a few milliseconds. The penetration of hot gases, produced by the combustion of the igniter near the front end of the gun barrel, into the void region leads to the ignition of solid granules by convective heating. The granule compaction and rapid pressurization are then set up during the subsequent ballistic cycle. The ignition front accelerates due to the resulting pressure build-up. The ignited propellants release hot gases which then move forward by the developed pressure gradient and thus ignite more propellants. As a consequence, a steep presure gradient is established inside the combustion chamber. These accelerated gaseous products finally cause the projectile to move. The flame spreading and possible shock-front formation in porous propellant charges are, without doubt, of importance in the design and analysis of propellant loading and combustion chamber configuration.

Numerical studies of the physics of combustion in a gun combustion chamber have been attempted in the past two decades. Most of the computer codes[2–5] were developed

within the context of a one-dimensional analysis. Recently, extension to multi-dimensional analysis for such problems has been made[6-8].

It is well established that the direct application of central-difference schemes to treat steep-front waves may cause numerical oscillations in regions having strong gradients during the ballistic cycle. The first-order accurate Lax scheme[9] offers positivity-preserving monotone solutions but sacrifices the solution accuracy near the high gradient region. Considerable numerical dissipation is added and it may sometimes lead to erroneous predictions of the real physics. Improvements on the solution accuracy can be easily made by using a higher-order discretization scheme, such as the Lax-Wendroff scheme[10], but this usually produces oscillatory solutions in regions with flow discontinuities. Accuracy and positivity seem to be contradictory to each other and mutually exclusive. This difficulty is a crucial issue and is directly related to the solution quality. It motivated researchers to develop a high-order non-oscillatory solution method for capturing shock-like solutions. Historically, a large number of high resolution schemes[11-13] have been developed and successfully applied to circumvent the above-mentioned numerical difficulties. For a further discussion of modern advection schemes the reader is referred to[14]. The present study focuses on the FCT technique. The idea behind FCT is to combine a high-order scheme with a low-order scheme in such a way that the high-order scheme is employed in regions where the variables under consideration vary smoothly, whereas in regions where the variables vary abruptly these two schemes are combined through a nonlinear combination of diffusive and anti-diffusive fluxes. The resulting discretized equations can maintain the positivity-preserving property.

In the following sections, a detailed theoretical formulation of the physical processes is first given, followed by a brief description of the FCT scheme employed. Finally, the analysis is applied to study the two-phase chemically reacting flow in a gun combustion chamber with a moving projectile.

2. FORMULATION

The numerical prediction of transient combustion processes in a granular-propellant bed is made by solving the following conservation equations for a two-phase mixture. These equations are formulated by assuming the gas and solid phases are interdispersed and coupled through appropriate interactions. Each phase is treated as a continuum. The conservation of mass, momentum, and energy for the gas and solid phases can be represented by the following expressions:

Gas phase

$$\frac{\partial}{\partial t}(\rho_1 R_1 \phi) + \frac{\partial}{\partial x}(\rho_1 R_1 u_1 \phi) = S_1 \tag{1}$$

Solid phase

$$\frac{\partial}{\partial t}(\rho_2 R_2 \phi) + \frac{\partial}{\partial x}(\rho_2 R_2 u_2 \phi) = S_2 \tag{2}$$

Table 1 Dependent variables and source terms of the gas and solid phase equations

	Gas phase		*Solid phase*	
	ϕ	S_1	ϕ	S_2
Mass	1	$\dot{m}_{comb}$	1	$-\dot{m}_{comb}$
Momentum	u_1	$-R_1\frac{\partial P}{\partial x}-D+\frac{4}{3}\frac{\partial}{\partial x}\left(\mu R_1\frac{\partial u_1}{\partial x}\right)+\dot{m}_{comb}u_2$	u_2	$-R_2\frac{\partial P}{\partial x}+D-\dot{m}_{comb}u_2-a_P^2R_c\frac{\partial}{\partial x}\left(\rho_2\frac{R_c-R_2}{R_1}\right)sgn(R_c-R_1)$
Energy	E_1	$-\frac{Q}{A}+\dot{m}_{comb}\left(E_{ch}+\frac{u_2^2}{2gJ}\right)-\frac{Du_2}{J}-\frac{1}{J}\frac{\partial}{\partial x}(R_1pu_1)$	E_2	$\frac{Q}{A\rho_2}$

where R_1 is the porosity of the gas and $R_1+R_2=1$. The dependent variables and source terms S in the above equations are given in Table 1.
The Nobel-Abel equation is used as the equation of state for the gas phase[1],

$$P=\left(\frac{1}{\rho}-b\right)^{-1}RT \tag{3}$$

where R is the specific gas constant and b is the co-volume. The constitutive equations used for the closure of equations (1) and (2) are described below.

Intergranular stress

The intergranular stress arises in a packed barrel in which the particles are agglomerated. This isotropic normal stress in the solid phase affects the particles only and is determined by the following correlation.[6]

$$\begin{aligned}\tau&=0 \qquad ; \quad 0\leqslant R_c\leqslant R_1\\ \tau&=a^2\rho_2R_c\frac{R_c-R_2}{R_1R_2}; \quad R_1\leqslant R_c\end{aligned} \tag{4}$$

where a is the speed of sound in the solid phase. There is no direct contact between particles when the porosity exceeds a critical value R_c.

Interphase drag

The average steady-state interphase drag D in the momentum equations is represented by the following correlation for a packed bed:

$$D=R_2\frac{S}{V}F \tag{5}$$

where $S = \pi r_p^2$ and $V = 4/3\pi r_p^3$ are the surface area and volume of a spherical particle, respectively. The interphase drag per unit area F of the solid phase can be modeled by Ergun's correlation:[15]

$$F = \frac{\rho|u-u_p|(u-u_p)\hat{f}}{6} \tag{6a}$$

where

$$\hat{f} = \begin{cases} 1.75 & \text{for} \quad R_1 \leqslant R_c \\ 1.75\left[\dfrac{R_2 R_c}{R_1(1-R_c)}\right] & \text{for} \quad R_c < R_1 \leqslant R_l \\ 0.3 & \text{for} \quad R_l < R_1 < 1 \end{cases} \tag{6b}$$

$$R_1 = \left[1 + 0.01986\left(\frac{1-R_c}{R_c}\right)\right]^{-1} \tag{6c}$$

In this study, $\hat{f}$ is taken to be 1.4 for the sake of simplicity.

Particle burning rate

An empirical pressure-dependent burning law is employed to model the particle surface regression rate under the steady-state condition:[8]

$$\dot{Z} = BP^n \tag{7}$$

where the constant B and pressure exponent n are specified for each propellant under investigation. The mass burning rate of propellant is given by

$$\dot{m}_{\text{comb}} = R_2 \rho_2 \frac{\dot{V}}{V} \tag{8}$$

where $\dot{V}/V$ is the fractional rate of change in propellant-grain volume. As far as the number of burning grains in each cell N and the number of perforations in each grain f are concerned, the propellant mass burning rate in each cell is given by

$$\Delta \dot{m}_{\text{comb}} = R_2(t)\rho_2(t)\Delta V(t) \tag{9}$$

where

$$\Delta V(t) = \frac{\pi}{4}(D_0^2 - fD^2)L - \frac{\pi}{4}(L-\beta(t))[(D_0-\beta(t))^2 - f(D_i+\beta(t))^2] \tag{10a}$$

$$\beta(t) = 2\dot{Z}\Delta t \tag{10b}$$

Gas-solid interphase heat transfer

The interphase heat transfer Q, arising from the propellant heating, is given by

$$Q = Sh_t \Delta T \tag{11}$$

where $h_t = Nuk/d$ is the total heat transfer coefficient and $d = 6V/S$ is the equivalent propellant grain diameter. The Nusselt number Nu is given by[3].

$$\mathrm{Nu} = \mathrm{Max}\left(1.8 \times 10^{-4} \frac{d}{k} P^{0.65}, 0.3 R_e^{0.62},\right) \tag{12}$$

where the dimension of pressure is MPa.

Molecular transport properties

Sutherland's law is used to compute both molecular viscosity and thermal conductivity. They are assumed to be functions of temperature and are given by[8].

$$\mu = \frac{C_1 T^{3/2}}{C_2 + T} \tag{13a}$$

$$k = \frac{C_3 T^{3/2}}{C_4 + T} = \frac{C_P}{P_r}\mu \tag{13b}$$

where

$$C_1 = 0.7535 * 10^{-6}\ \mathrm{lbm/ft} - s - \sqrt{R}, \quad C_2 = 262.5R,$$

$$C_3 = 0.291 \times 10^{-6}\ \mathrm{Btu/ft} - s - R^{3/2},$$

$$C_4 = 170.1\,R, \quad Pr = \frac{4\gamma}{9\gamma - 5}, \quad \gamma = 1.27.$$

3. NUMERICAL MODEL

For the sake of simplicity in describing the presently employed discretization scheme, equations (1) and (2), written in terms of the strong conservation law form, can be further expressed in the following symbolic form:

$$\frac{\partial \underline{q}}{\partial t} + \frac{\partial \underline{F}}{\partial x} = \underline{S} \tag{14}$$

Apart from the nonlinearity in the above partial differential equation, it is particularly challenging to analyze a problem involving reaction process. In the combustion chamber, a shock-like high gradient profile over an extremely short distance may be formed, even if the computation begins with a smooth initial condition, due to the energy input through the release of chemical potential. Consequently is important in the present two-phase flow simulation to adopt a discretization scheme capable of capturing accurate but non-oscillatory solutions.

Godunov[16] has clearly demonstrated that there is no linear high-order method which guarantees monotonicity. In this regard, it is inevitable to adopt a nonlinear discretization method. A large number of monotone discretization methods for equation (14), are available[14] We can divide them into three categories, namely linear hybridization methods, methods based on Godunov's algorithm[16], total variational diminishing (TDV) methods[11]. Among these, the flux corrected transport (FCT) algorithm, classified in the first category, is the only one that is applicable to multidimensional analysis[17]. Based on the premise that the present one-dimensional scheme can be extended to the multi-dimensional analysis, we have adopted the FCT technique in the present analysis.

In linear hybridization, such as the FCT technique, the results of a low-order method and a high-order method are blended in a nonlinear fashion. We first discuss these two basic schemes as follows:

3.1 *Low-order discretization scheme*

We adopt the first-order Lax method[9] to guarantee positivity, which is very desirable when sharp gradients (or discontinuities) are captured as part of the solution. In the Lax method, the solution is expanded in a Taylor series about point (x, t) only to the first two terms and the time derivative are rearranged. This, together with the use of centered differences for the remaining spatial derivatives, yields the following explicit discretized equation

$$\underline{q}_j^{n+1} = \frac{1}{2}\left[(\underline{q}_j^n + \underline{q}_{j-1}^n) - \frac{\Delta t}{\Delta x}(\underline{F}_{j+1}^n - \underline{F}_{j-1}^n)\right] + \underline{S}_j^n \Delta t \tag{15}$$

3.2 *High-order discretization method*

To assure accuracy, we adopt an high-order method in smooth regions exclusively. The Lax-Wendroff method[10] was developed in the same vein as the Lax method by a Taylor series expansion. For attaining greater accuracy, we include the second derivative term $(\Delta t^2/2)\ (\partial^2 \underline{q}/\partial t^2)|_{x,t}$ in the expansion. Replacing the time derivative with the spatial derivative through (14) yields

$$\underline{q}_{tt} = \underline{S}_t - (\underline{A}\ \underline{S})_x + (\underline{A}\ \underline{F}_x)_x \tag{16}$$

where the Jacobian matrix $\underline{A}$ is defined by $\underline{A} = \partial \underline{F}/\partial \underline{q}$.

Using central differencing, the high-order scheme based on the Lax-Wendroff scheme is derived to be

$$\underline{q}_j^{n+1} = \underline{q}_j^n - \frac{1}{2}\left\{\frac{\Delta t}{\Delta x}(\underline{F}_{j+1}^n - \underline{F}_{j-1}^n) + \left(\frac{\Delta t}{\Delta x}\right)^2 [\underline{A}_{j+1/2}^n(\underline{F}_{j+1}^n - \underline{F}_j^n) - \underline{A}_{j-1/2}^n(\underline{F}_j^n - \underline{F}_{j-1}^n)]\right\}$$

$$-\frac{1}{2}\frac{\Delta t^2}{\Delta x}[\underline{A}_{j+1/2}^n(\underline{S}_{j+1}^n - \underline{S}_j^n) - \underline{A}_{j-1/2}^n(\underline{S}_j^n - \underline{S}_{j-1}^n)] \tag{17}$$

The Jacobian matrix at the $j + 1/2$ location is evaluated by

$$\underline{A}_{j+1/2} = \underline{A}\left(\frac{\underline{q}_j + \underline{q}_{j+1}}{2}\right) \tag{18}$$

We denote the Lax-Wendroff solution by $\underline{q}^{**}$.

The first-order accurate Lax scheme is extremely diffusive to maintain positivity and monotonicity. The second-order accurate Lax-Wendroff scheme is less diffusive but is susceptible to instability in the vicinity of a sharp gradient. To circumvent these problems, we incorporated a nonlinear monotone mechanism into the formulation so that the respective advantages of the Lax and Lax-Wendroff methods can be combined. The flux corrected transport technique of Boris and Book[13], consists of the following steps to compute the fluxes at cell surfaces $j + 1/2$, for example, from the Lax and Lax-Wendroff solutions.

(i) Generate diffusive fluxes:

$$\underline{f}_{j+1/2}^d = V_{j+1/2}(\underline{q}_{j+1}^n - \underline{q}_j^n) \tag{19}$$

where $V_{j+1/2}$ is the diffusive coefficient defined as

$$V_{j+1/2} = \frac{1}{6} + \frac{1}{3}\left[\frac{1}{2}(u_j + u_{j+1})\frac{\Delta t}{\Delta x}\right]^2 \tag{20}$$

(ii) Generate anti-diffusive fluxes:

$$\underline{f}_{j+1/2}^{ad} = \mu_{j+1/2}(\underline{q}_{j+1}^{**} - \underline{q}_j^{**}) \tag{21}$$

where μ is the anti-diffusion coefficient defined as

$$\mu_{j+1/2} = \frac{1}{6} - \frac{1}{6}\left[\frac{1}{2}(u_j + u_{j+1})\frac{\Delta t}{\Delta x}\right]^2 \tag{22}$$

(iii) Limit the anti-diffusie fluxes:

To obtain a positivity-preserving algorithm, the anti-diffusive fluxes in step (ii) are modified by a flux-correction process. The corrected fluxes are chosen in a nonlinear manner to prevent the anti-diffusive stage from introducing new maxima or minima in

the solution.

$$T = sgn(f^{ad}_{j+1/2}) \tag{23}$$

$$f^{cad}_{j+1/2} = T \cdot \max[0, \min\{T\Delta q^{***}_{j-1/2}, |f^{ad}_{j+1/2}|, T\Delta q^{***}_{j+3/2}\}] \tag{24}$$

where

$$q^{***}_j = q^{**}_j + f^{d}_{j+1/2} - f^{d}_{j-1/2}, \Delta q^{***} = q^{**}_{j+1} - q^{***}_j.$$

(iv) The values of q_j are given by

$$q^{n+1}_j = q^{***}_j - f^{cad}_{j+1/2} + f^{cad}_{j-1/2} \tag{25}$$

4. COMPUTED RESULTS

In Figure 1, we define the computational domain as the region between the breech and the projectile, which is divided into 100 non-uniform cells. In the course of the chamber pressurization, the solution domain is expanded as the force acting on the projectile exceeds the spindle force and results in the movement of the projectile. The basepad as well as the center-core igniter normally consist of black powder. A jet of hot gases is discharged from a primer, taken to be 16.67% of the length of the chamber, to ignite the basepad and then, in turn, ignite the center-core igniter. The ignition sequence is modelled by specifying the flow rate and energy. In this study, a bag of M6 propellants is considered to be uniformly distributed. The initial density of the solid propellant is assumed to be 98.5 lbm/ft^2. The propellant ignites as its surface temperature exceeds the ignition temperature, $T_{ign} = 450$ K. For the sake of clarity, the input data is summarized in Table 2.

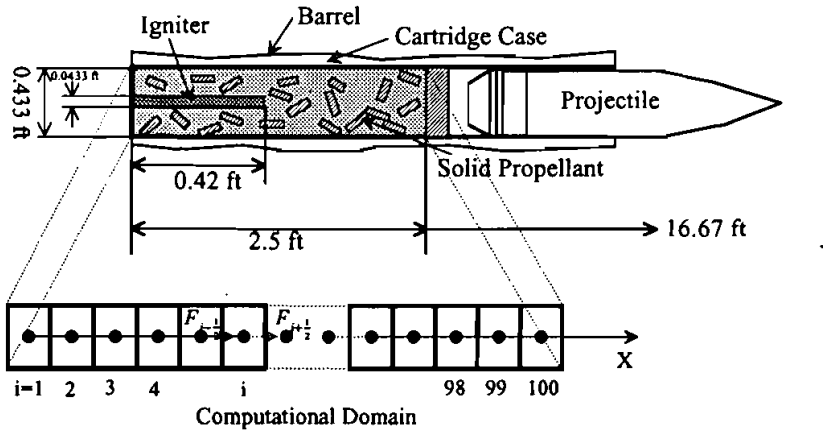

Figure 1 Schematic of a mobile granular propellant bed.

Table 2 Input data

Gun Tube	Diameter	0.433 ft, (constant)
	Breech Face	0.0 cm
	Propellant Bed	2.5 ft
	Muzzle	19.17 ft
	Surface Temperature	535 R
Projectile	Mass	100 lbm
	Density	500 lbm/ft^3
	Elastic Stress Wave	160000 ft/sec
Propellant	Total Mass	21 lbs
	Density	98.5 lbm/ft
	Grain Length	0.0833 ft
	Grain Diameter	0.0375 ft
	Perforation	0.00375 ft
	Burn rate	Bp cm/sec
	B	0.2218; p in MPa
	n	0.7864 (constant)
	Ignition Temperature	810 R
	Thermal Conductivity	0.356E-4 Btu/ft-see-R
	Thermal Diffusivity	0.935E-6 ft/sec
	Emissivity	0
	Chemical Energy	1607 Btu/lbm
	Molecular Weight	21.36
	Co-volume	0.0173611 ft/lbm
	Plastic Deformation Stress wave	1900 ft/sec
	Elastic Stress Wave	3800 ft/sec
	Porosity	0.4217 (constant)
	Ultimate Failure Stress	1.584E6 lbf/ft
	Yield Stress	8.21E5 lbf/ft
	Initial Temperature	535 R
Igniter (Black Powder)	Chemical Energy	675 Btu/lbm
	Molecular Weight	36.13
	Diameter	0.00433 ft
	Co-volume	0.016493055 (constant)
	Thermal Conductivity	0.2E-4 Btu/ft-sec-R
	Thermal Diffusivity	1.0E-6 ft/see
Initial Conditions	Ambient Air Temperature	535 R
	Ambient Air Pressure	2116.8 lbf/ft^2
	Propellant Bed Temperature	535 R
	Velocity	0.0 ft/see

Figure 2 shows the calculated pressure distributions at various times. The initial length of the propellant bed is 2.5 ft. Because of its highly dissipative nature the Lax method fails to produce physically accurate solutions. The calculated pressure distribution is rather uniform during the entire event; no wave propagation phenomenon is observed. In view of this, the following discussion is based on the Lax-Wendroff method with the FCT correction.

Owing to the penetration of the igniter gases into the propellant bed, the granular propellants near the breach end ignite first, and their combustion products cause a local pressure increase at $t = 2$ msec. The pressure wave and its associate flame then propagate downstream to the projectile base. At this time, the projectile starts to move since the force acting on the projectile exceeds the friction between the gun barrel and the projectile. As time elapses, the combustion chamber volume increases because of the movement of the projectile, thereby causing a pressure decrease starting at

$t = 5$ msec. The computed pressure and flame fronts are presented in Figure 3, which provide useful information regarding wave propagation in the gun tube. The calculated gas-phase velocity distributions at various times are shown in Figure 4. According to the pressure profiles given in Figure 2, a vigorous combustion of the granular propellant occurs near the projectile base at t = 3 msec. The pressure gradient established in the chamber causes a negative gas velocity, with combustion gases moving upstream toward the breech end. Figure 5 presents the distributions of the solid-particle velocity. The lag of the velocity with respect to its counterpart in the gas phase is clearly observed.

The gas-phase temperature is also calculated, since it influences the combustion of granular propellants. The flame spreading during the initial development of the combustion process is clearly observed in Figure 6. The maximum temperature takes place at the breach end at t = 3 msec. This may be attributed to the temperature recovery effect at that (stagnation) point. The temperature distribution then becomes more uniform as the projectile moves downstream. Figure 7 shows the calculated gas density distributions.

Finally, the gas-phase volume fraction is calculated, giving the result shown in Figure 8. This result serves as a guideline to examine the extent of the solid propellant

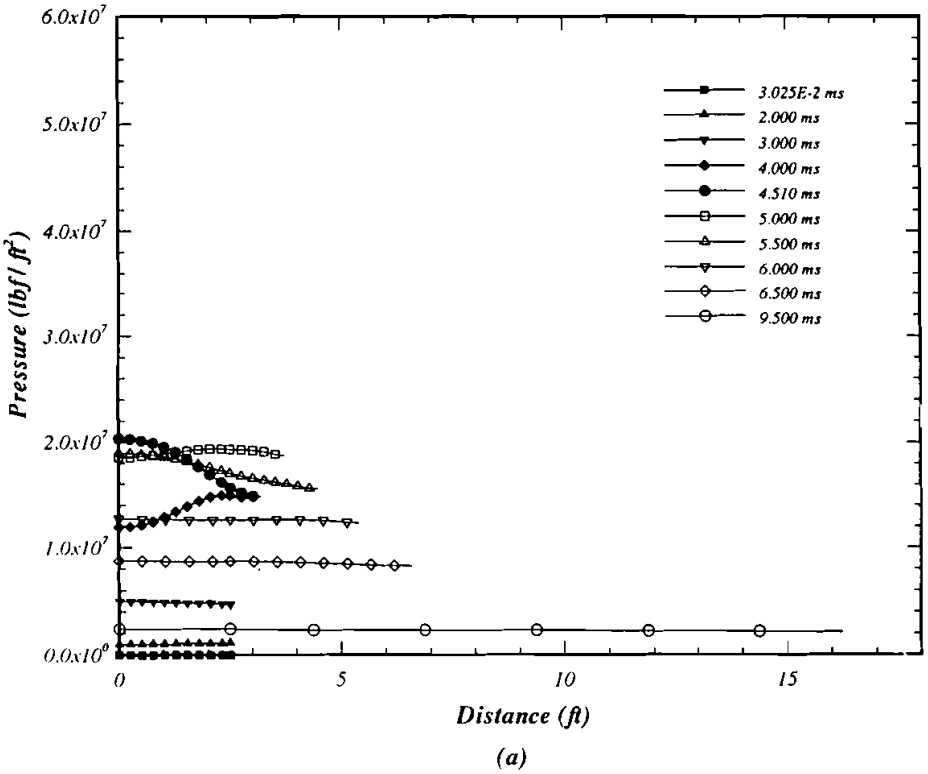

(a)

Figure 2 Pressure distributions in the gun barrel at various times: (a) Lax method, (2) Lax-Wendroff method with FCT correction.

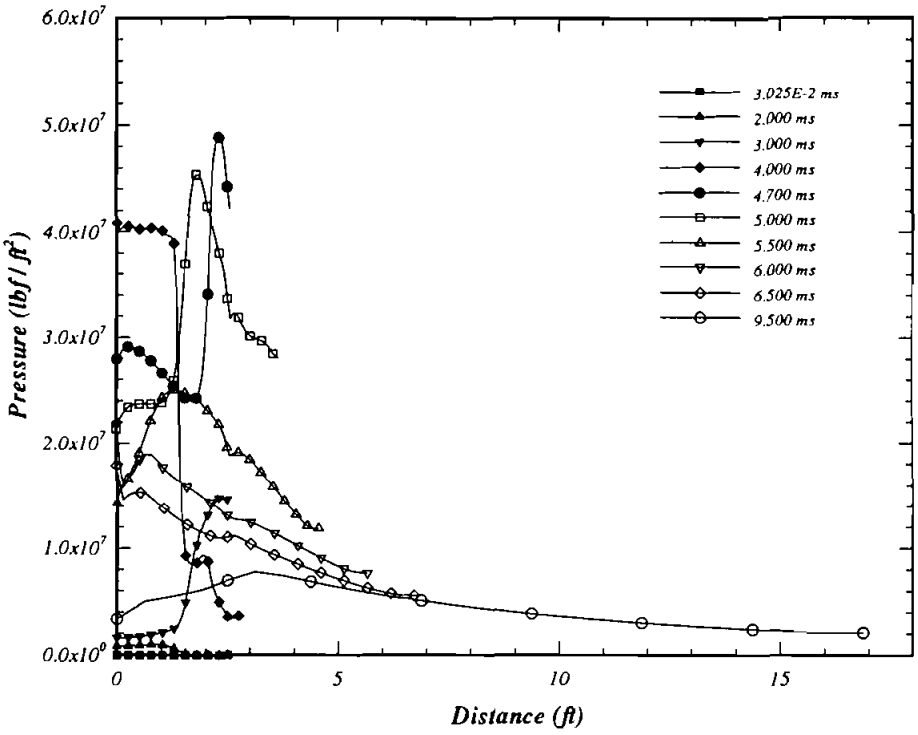

(b)

Figure 2 *(Continued)*

burning. A rapid increase of the gas-phase volume takes place near the forward end due to the burning and forward motion of the solid particles, especially in the early stage of the ballistic cycle. It is interesting to note that in the later phase of the combustion event, the transient compaction of the granular propellant bed near the projectile base causes a reduction of the gas-phase volume. Finally, the gas volume fraction becomes unity when the propellant is completely burned.

5. CONCLUSIONS

A numerical simulation of the gas-solid flowfield in a gun tube is presented in this paper. The global trend of the combustion physics has been well predicted by the present computer code. The main conclusions regarding the computational aspect are summarized as follows.

1. A monotone, positivity-preserving algorithm is indispensable in predicting the two-phase combustion in gun interior ballistics since an abrupt change in thermal as well as flow properties may occur. A high resolution solution was made possible by adding an anti-diffusive flux. To maintain the positivity of the solution a limiter limiting

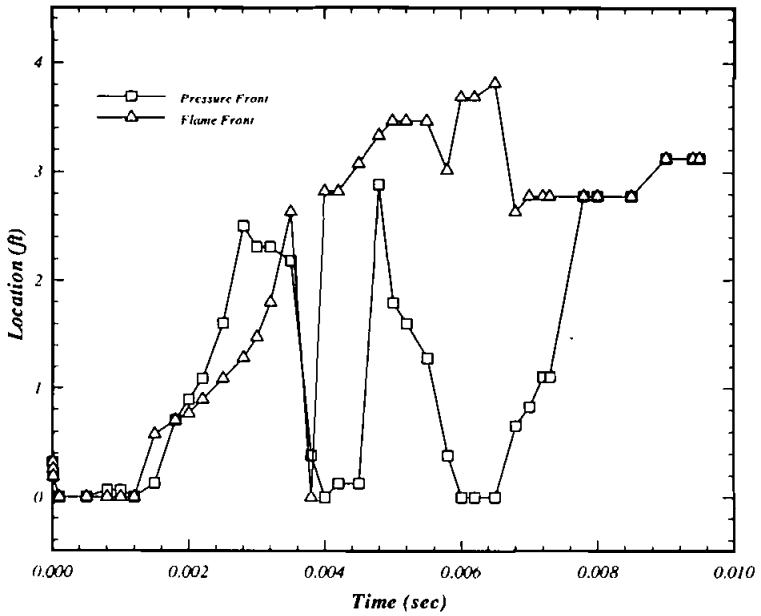

Figure 3 Time histories of pressure and flame fronts.

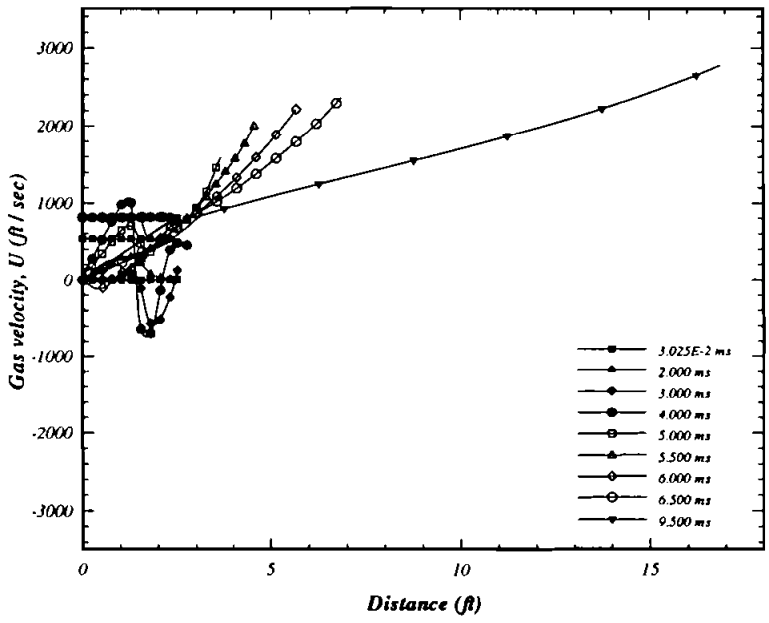

Figure 4 Distributions of the gas-phase velocity at various times.

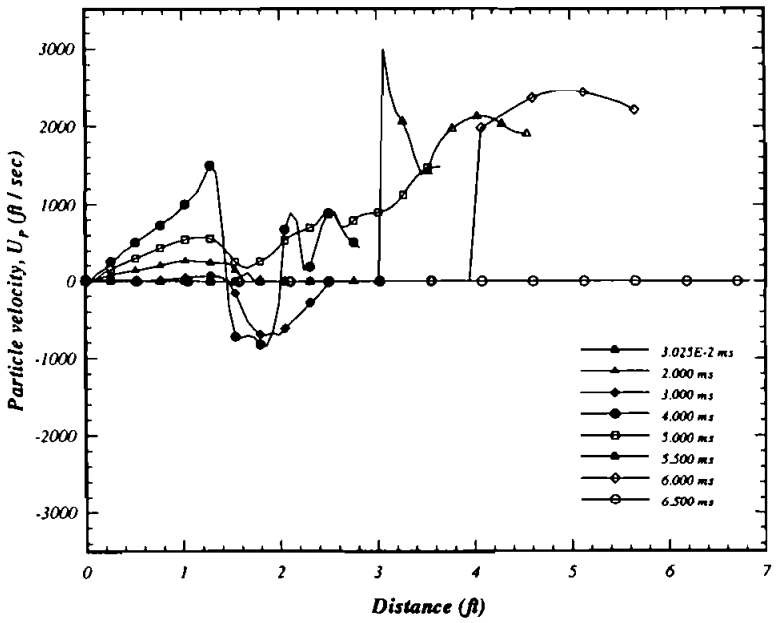

Figure 5 Distributions of the solid-particle velocity at various times.

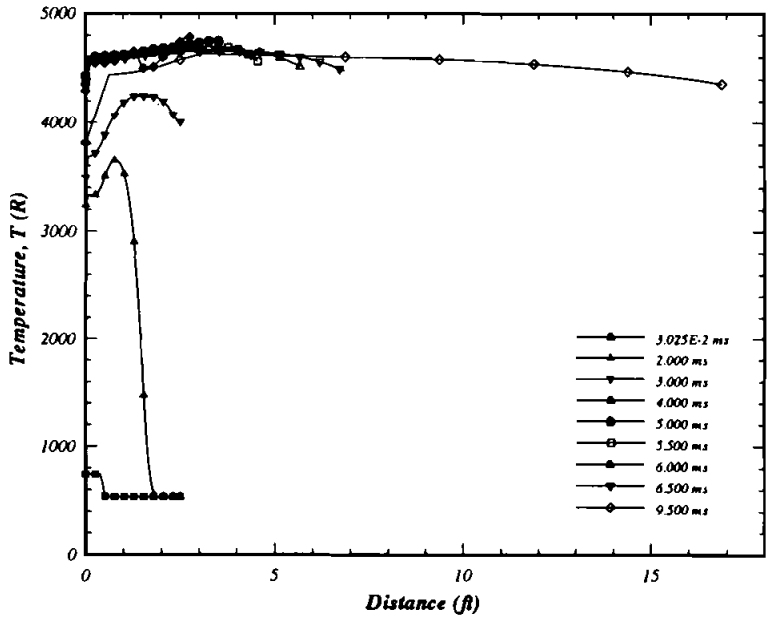

Figure 6 Distribution of the gas-phase temperature at various times.

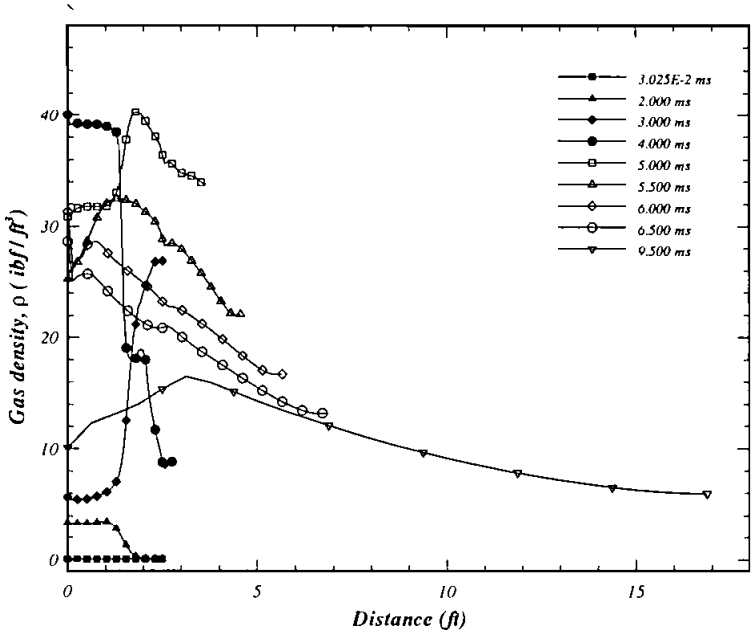

Figure 7 Distribution of the gas-phase density at various times.

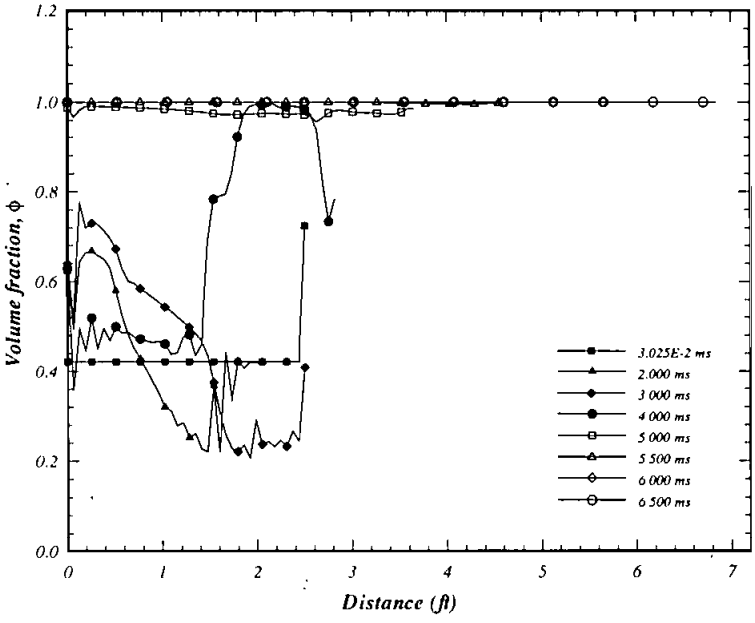

Figure 8 Distribution of the gas-phase volume fraction at various times.

must be incorported in the solution algorithm to ensure that no new maxima or minima will be computed.

2. A low-order solution which must be strongly diffused to ensure positivity is crucial to the implementation of the FCT nonlinear filtering technique.

Acknowledgments

This research was conducted under a contract sponsored by the National Science Council. Thanks are expressed to Mr. H-C Cheng, Director of the Ballistic Research Center of the Combined Service Force, and his colleagues who made this project possible.

References

1. Kuo, K. K. (1986) *Principles of Combustion*, John Wiley and Sons, New York.
2. Kuo, K. K., Koo, J. H., Davis, T. R., and Coates, G. R. (1976) "Transient Combustion in Mobile Gas-Permeable Propellants", *Acta Astronautics*, **3**, 573–591.
3. Fisher, E. B., and Graves, K. W. (1972) "Mathematical Model of Double Base Propellant Ignition and Combustion in the 81 mm Mortar", Calspan Report No. GD-3029-D-1, Aug.
4. Gouh, P. S. (1977) "Numerical Analysis of a Two-Phase Flow with Explicit Internal Boundaries", IHCR 77-5, Naval Ordnance Station, Indian Head, MD, April.
5. Markatos, N. C. (1986) "Modelling of Two-Phase Transient Flow Combustion of Granular Propellants", *Int. J. of Multiphase Flow*, **12** (6), 913–933.
6. Gough, P. S. (1979) "Two-Dimensional Convective Flame Spreading in Packed Beds of Granular Propellant", ARBRL-CR-00404, July.
7. Gibeling, H. J., Buggeln, R. C. and McDonald, H. (1980) "Development a Two-Dimensional Implicit Interior Ballistics Code", ARBRL-CR-00411, January.
8. Markatos, N. C. and Kirkcaldy, D. (1983) "Analysis and Computation of Three-Dimensional Transient Flow and Combustion Through Granulated Propellants", *Int. J. of Heat Transfer*, **26** (7), 1037–1053.
9. Lax, P. D. (1954) "Weak Solutions of Nonlinear Hyperbolic Equations and Their Numerical Computation", *Comm. of Pure and Appl. Math.*, **7**, 159–193.
10. Lax, P. D. and Wendroff, B. (1960) "Systems of Conservation Laws", *Comm. of Pure Appl. Math.*, **31**, 217–237.
11. Harten, A. (1983) "High Resolution Schemes for Hyperbolic Conservation Laws", *J. of Comput. Phys.*, **49**, 357–393.
12. Harten, A. and Osher, S. (1987) "Uniformly High-Order Accurate Non-Oscillatory Schemes", *SIAM J. of Number. Analysis*, **24** (2), 231–303.
13. Boris, J. P. and Book, D. L. (1973) "Flux Corrected Transport I: SHASTA, A Fluid Transport Algorithm That Works", *J. of Comput. Phys.*, **11**, 38–69.
14. Oran, E. S. and Boris, J. P. (1987) *Numerical Simulation of Reactive Flow*, Elsevier Science Publishing Co. Inc.
15. Ergun, S. (1952) "Fluid Flow Through Packed Columns, Chemical Engineering Progress", **48**, 89.
16. Godunov, S. K. (1959) "Finite Difference Methods for Numerical Computation of Discontinuous Solutions of the Equations of Fluid Dynamics", Mat, Sb. **47**, 271–306.
17. Lohner, R., Morgan, K., Peraire, J. and Vahdati, M. (1987) "Finite Element Flux-Corrected Transport (FEM-FCT) for Euler and Navier-Stokes Equations", *Int. J. for Numer. Methods in Fluids*, **7**, 1093–1109.